Original Article

Multimodal ultrasound imaging for diagnostic differentiation of sclerosing adenosis from invasive ductal carcinoma

Wen Li[1,2#], Yan Zheng[1#], Haizhen Liu[2#], Zhengling Tai[2], Huihui Zhu[2], Zhaoxi Li[2], Qinghua Gu[3], Yonggang Li[1,4,5]

[1]Department of Radiology, The First Affiliated Hospital of Soochow University, Suzhou, China; [2]Department of Ultrasound, Huadong Sanatorium, Wuxi, China; [3]Department of Radiology, Suzhou Yongding Hospital, Suzhou, China; [4]Institute of Medical Imaging, Soochow University, Suzhou, China; [5]National Clinical Research Center for Hematologic Diseases, the First Affiliated Hospital of Soochow University, Suzhou, China

Contributions: (I) Conception and design: Y Li, W Li; (II) Administrative support: Y Li, Q Gu, Z Li; (III) Provision of study materials or patients: Y Zheng, H Liu, W Li; (IV) Collection and assembly of data: H Liu, W Li, H Zhu, Z Tai; (V) Data analysis and interpretation: H Liu, H Zhu, Z Tai; (VI) Manuscript writing: All authors; (VII) Final approval of manuscript: All authors.

[#]These authors contributed equally to this work as co-first authors.

Correspondence to: Yonggang Li, MD, PhD. Department of Radiology, The First Affiliated Hospital of Soochow University, 188 Shizi Street, Suzhou 215006, China; Institute of Medical Imaging, Soochow University, Suzhou 215000, China; National Clinical Research Center for Hematologic Diseases, the First Affiliated Hospital of Soochow University, Suzhou 215000, China. Email: liyonggang224@163.com; Qinghua Gu, MS. Department of Radiology, Suzhou Yongding Hospital, 1388 Gaoxin Road, Wujiang District, Suzhou 215200, China. Email: 335092646@qq.com; Zhaoxi Li, BS. Department of Ultrasound, Huadong Sanatorium, 67 Jingyuan Road, Binghu District, Wuxi 214063, China. Email: 13812183596@163.com.

Background: Sclerosing adenosis (SA) is a common proliferative benign lesion without atypia in the breast that may mimic invasive ductal carcinoma (IDC) on medical imaging, leading to it often being misdiagnosed and mistreated. Consequently, the purpose of this study was to assess the diagnostic value of multimodal ultrasound imaging in distinguishing SA from IDC.

Methods: Multimodal ultrasound imaging, including automated breast volume scan (ABVS), elasticity imaging (EI), and color Doppler flow imaging (CDFI), were performed on 120 consecutive patients comprising 122 breast lesions (54 SA, 68 IDC). All lesions were pathologically confirmed. Multimodal ultrasound imaging features were compared between the two groups. Binary logistic regression analysis based on ABVS, EI, and CDFI was conducted to formulate a logistic regression equation for differentiating SA from IDC. The diagnostic performances of ABVS, EI, CDFI, and their combination were compared by the receiver operating characteristic (ROC) curve analysis.

Results: The sensitivity, specificity, and accuracy of ABVS, EI, CDFI, and their combination in differentiating SA from IDC were, respectively, 75.00%, 72.22%, and 73.77%; 86.76%, 72.22%, and 80.33%; 73.53%, 64.81%, and 69.67%; and 88.24%, 74.07%, and 81.97%. Combining multimodal ultrasound imaging yielded an area under the curve (AUC) of 0.895 (95% confidence interval: 0.827–0.943), which was higher than that of ABVS, EI, and CDFI, with AUC values of 0.736, 0.795, and 0.692, respectively, and the difference was statistically significant (ABVS *vs.* combined model, P<0.001; CDFI *vs.* combined model, P<0.001; EI *vs.* combined model, P<0.001). There was no significant difference in the diagnostic efficacy among the three imaging modalities (ABVS *vs.* EI, P=0.266; ABVS *vs.* CDFI, P=0.4671; EI *vs.* CDFI, P=0.051). Compared with those in IDC, the calcification (16.67% *vs.* 57.35%; P<0.001) and retraction phenomena in the coronal planes (18.52% *vs.* 57.35%; P<0.001) were less common in patients with SA, while circumscribed margin (38.89% *vs.* 5.88%; P<0.001), vascularity grade 0–I (64.81% *vs.* 26.47%; P<0.001), and elasticity scores 1–3 (72.22% *vs.* 13.24%; P<0.001) were more frequently found

in patients with SA. Patients with SA were significantly younger than were patients with IDC (43±11 *vs.* 54±11 years; P<0.001), and the lesion size was smaller in patients with SA than in those with IDC (median size 1.0 cm; interquartile range (IQR), 0.9 cm *vs.* median size 1.3 cm; IQR, 1.3 cm; P<0.001).

Conclusions: The preliminary results suggested that multimodal ultrasound imaging can improve the diagnostic accuracy of SA and provide additional information for differential diagnosis of SA and IDC.

Keywords: Sclerosing adenosis (SA); invasive ductal carcinoma (IDC); multimodal ultrasound imaging; automated breast volume scan (ABVS); elasticity imaging (EI); color Doppler flow imaging (CDFI)

Submitted Apr 17, 2023. Accepted for publication Nov 09, 2023. Published online Jan 02, 2024.
doi: 10.21037/qims-23-524
View this article at: https://dx.doi.org/10.21037/qims-23-524

Introduction

Sclerosing adenosis (SA) is a specific type of breast adenosis, which accounts for about 1.3–2% of all breast adenosis cases (1,2). The etiology of SA still remains elusive, but it may be associated with increased estrogen concentration (3). SA is typically asymptomatic or manifests as a palpable mass. However, it is discovered unexpectedly in women who have undergone imaging or histopathology examinations for other reasons (1). SA is a complex lesion and is pathologically characterized by epithelial, myoepithelial, and basement membrane proliferation (4). SA can form adenosis tumors and may be mistaken for invasive ductal carcinoma (IDC) due to the fact that the proliferative tissue squeezes the lobule to form a pseudo-infiltration (5). However, the clinical treatments for SA and IDC are significantly different. Therefore, in the era of precision medicine, it is essential to improve the assessment of SA in order to reduce the psychological burden on patients and enable clinicians to develop more rational treatment plans.

At present, preoperative diagnosis of SA is highly challenging, especially as it relates to differentiating SA from IDC (1,6). Although mammography (MG) and conventional ultrasound, the two most commonly used diagnostic techniques for breast diseases, have progressed consistently, it remains difficult to distinguish between SA and IDC based on imaging findings (7). Magnetic resonance imaging (MRI) is an important examination for breast diseases by virtue of its high-resolution determination of soft tissue (8). However, it is too expensive and time-consuming to be used as a routine examination for the diagnosis of SA (9).

In recent years, with the development of ultrasound techniques, multimodal ultrasound imaging has been applied in the detection of breast diseases in China. Previous studies (10,11) have shown that the application of some ultrasonic techniques that can provide comprehensive information about lesions, including grayscale, elastography, and color Doppler imaging, are beneficial for differentiating benign from malignant lesions. Wang *et al.* (12) demonstrated that the combined use of virtual touch tissue quantification (VTQ) and automated breast volume scanning (ABVS) has the potential to improve diagnostic accuracy and specificity, making it a promising ultrasound technique for the differential diagnosis of breast lesions. Li *et al.* (13) indicated that multimodal ultrasound could improve the specificity in Breast Imaging Reporting and Data System (BI-RADS) category 4 lesions and thus reduce unnecessary biopsies. However, only few studies have investigated multimodal ultrasound imaging for SA, especially based on ABVS, elasticity imaging (EI), and color Doppler flow imaging (CDFI) (1,14). Therefore, using a retrospective analysis, we test the hypothesis that multimodal ultrasound imaging (ABVS, EI, and CDFI) can provide more salient information and exhibit a greater diagnostic performance for the accurate differentiation of SA and IDC. We present this article in accordance with the STARD reporting checklist (available at https://qims.amegroups.com/article/view/10.21037/qims-23-524/rc).

Methods

The study was conducted in accordance with the Declaration of Helsinki (as revised in 2013) and was approved by the Institutional Review Board of the Huadong Sanatorium (approval No. ECHS2023-09). Individual consent for this retrospective analysis was waived.

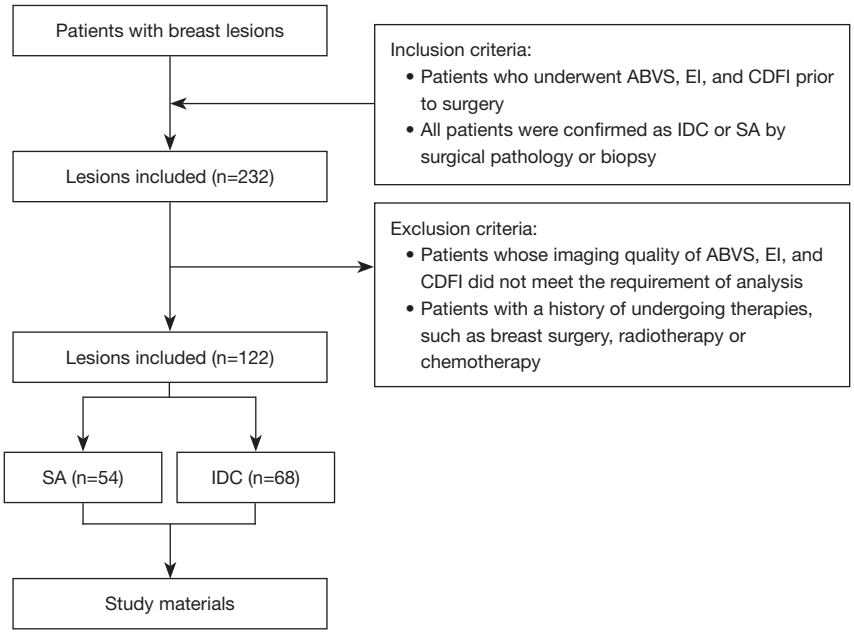

Figure 1 The flowchart of study participant selection. ABVS, automated breast volume scan; EI, elasticity imaging; CDFI, color Doppler flow imaging; IDC, invasive ductal carcinoma; SA, sclerosing adenosis.

Participants

Multimodal ultrasound features of 120 female patients (mean age 49±12 years), age range, 24–76 years) comprising 122 breast lesions who underwent ABVS, EI, and CDFI in Huadong Sanatorium from February 2018 to February 2021 were retrospectively reviewed. The inclusion criteria were as follows: (I) patients who underwent ABVS, EI, and CDFI prior to surgery; and (II) patients who were confirmed as IDC or SA via surgical pathology or biopsy. The exclusion criteria were as follows: (I) patients whose imaging quality of ABVS, EI, and CDFI did not meet the requirements of analysis; and (II) patients with a history of undergoing therapies, such as breast surgery, radiotherapy or chemotherapy. The selection process for the study participants based on the inclusion and exclusion criteria is shown in *Figure 1*. The eligible patients were divided as follows into two groups according to the results of pathological diagnosis: 54 patients with SA (mean age 43±11 years; age range, 24–69 years) and 68 patients with IDC (mean age 54±11 years; age range, 31–76 years).

Imaging acquisition

ABVS, EI, and CDFI were performed by sonographers with 8 years of experience in medical imaging using the ACUSON S2000 ABVS (Siemens Healthineers, Erlangen, Germany), which was equipped with a 5.5- to 18-MHz variable frequency transducer (18L6HD5) and a 15-cm-wide linear array transducer with a 5- to 14-MHz bandwidth.

ABVS

ABVS was performed after hand-held ultrasound (HHUS). Based on the location of the target lesions, all patients were placed in a supine or lateral position. The scanning included anterior-posterior, lateral, and medial orientations. Additional inferior and superior section scans were performed on larger breasts. The collected data were then transferred to the ABVS workstation to obtain basic planar images, and a three-dimensional reconstruction of the entire breast, including images on the vertical and coronal planes, was performed using these images. Image analysis in ABVS was essentially based on the evaluation of same image features as those for HHUS and included shape, margin, orientation, echo pattern, posterior echogenicity, and calcification according to the BI-RADS lexicon (15). The diagnostic criteria were as follows: (I) malignant masses were defined as irregularly shaped masses with a spiculated margin or echogenic halo; (II) solid masses with one of

three suspicious findings (microcalcifications, no parallel orientation, or no circumscribed margin) were classified as benign, while solid masses with two or more suspicious findings were classified as malignant; (III) for nonmass-like lesions, localized hypoechoic areas with one of three suspicious findings (ductal change, segmental distribution, or microcalcifications) were considered benign, whereas localized hypoechoic areas with two or three suspicious findings were considered malignant (16).

CDFI

After completion of the ABVS examination, CDFI was carried out through choosing the optimal grayscale ultrasound image. In order to minimize disruption, patients were told to breathe quietly and avoid swallowing during the imaging process.

Adjustments were made to Doppler sonographic parameters in order to detect low velocities. In particular, the lowest pulse repetition frequency (PRF) and Doppler gain settings that did not result in aliasing were used; the PRF was 500–800 Hz with 70–80% color gain, and the wall filter was set to 25–50 Hz. With a limited field of view, the color box was kept in the area of interest and kept as small as possible to maintain a high frame rate. A vessel was defined as a linear or punctuated colored signal that was not associated with adjacent color noise (it is essential to optimize the color gain setting to reduce artifacts). In the case of skin abnormalities, a substantial amount of gel was applied without the use of a stand-off pad. The lesions were then categorized as follows based on the vascular pattern described by Adler *et al.* (17): absent, grade 0; minimal, grade I, one or two pixels containing flow (<0.1 cm in diameter) were observed; moderate, grade II, three or few small vessels and/or a main vessel were observed; marked, grade III, four or more vessels were observed.

EI

After CDFI examination, EI was performed in routine fashion. During the examination, slight pressure was applied on patients' breast, and then images were acquired until the quality reached a value of 50. The selection of the sampling frame was carried out on the basis of both the target lesion and surrounding tissues. Differences in hardness of the region of interest (ROI) could be reflected by the color map (blue was representative of harder tissue, and green was indicative of softer tissue). Elastic scores were classified into five different classes as follows (18): (I) elastic score 1, the nodule was displayed homogeneously in green; (II) elastic score 2, the nodule was displayed predominantly in green with few blue spots; (III) elastic score 3, the nodule was displayed with 50% of areas in blue and green; (IV) elastic score 4, the nodule was displayed homogeneously in blue; and (V) elastic score 5, the nodule and surrounding tissues were displayed homogeneously in blue.

To eliminate interobserver variation, two radiologists (with 8 and 10 years of experience, respectively) who were blinded to the clinical data of the patients captured the sonographic characteristics; any discrepancies were resolved by consulting a third expert with 15 years of experience.

Statistical analysis

Statistical analysis was performed using SPSS 22.0 (IBM Corp., Armonk, NY, USA) and MedCalc 19.0.7 (MedCalc Software Ltd., Ostend, Belgium) software. Normally distributed quantitative data (e.g., age) are expressed as mean ± standard deviation (SD) and were compared with the Student's *t*-test. Abnormally distributed quantitative data (e.g., lesion size) are expressed as the median with interquartile range and were compared with the Mann-Whitney test. The χ^2 test or the Fisher exact test was used to analyze categorical variables (e.g., ultrasound imaging characteristics). Binary logistic regression analysis based on three imaging modalities (ABVS, EI, and CDFI) was conducted to formulate the following logistic regression equation: logit (P) = $\alpha \times$ ABVS + $\beta \times$ EI + $\gamma \times$ CDFI + constant, where α, β, and γ are the regression coefficients. Receiver operating characteristic (ROC) curve analysis was performed to evaluate the diagnostic performance of ABVS, EI, CDFI, and their combination. *Z* test was used to calculate and compare the area under the curve (AUC) values for each method. The reported statistical significance levels were all two-sided, and a P value <0.05 was considered significant.

Results

Pathological diagnosis

Among 54 lesions, there were 19 pure SA lesions and 35 SA lesions combined with benign lesions, including 16 cases with cyclomastopathy, five cases with adenoma fibrosum, six cases with intracanalicular papilloma, and eight cases with metaplasia apocrine.

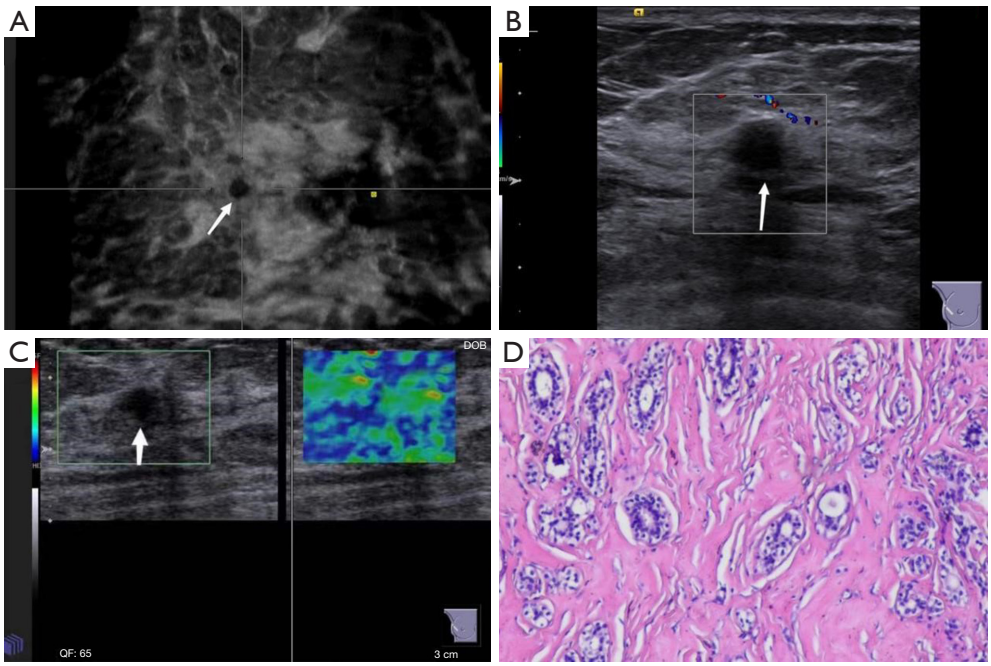

Figure 2 Pictures shows the imaging and histopathology findings of a case of sclerosing adenosis. (A) An SA lesion (white arrow) with a regular shape, circumscribed margin, and no retraction phenomenon in the coronal planes. (B) CDFI shows a lesion (white arrow) absent of blood flow. (C) The lesion's (white arrow) elasticity imaging shows a color code pattern of central blue surrounded by green, indicating its stiffness, distribution with an elasticity score of 3. (D) HE staining showing an SA lesion characterized by compressed and crowded glandlike acini with the proliferation of distorted stromal fibrosis (HE staining; original magnification 100×). SA, sclerosing adenosis; CDFI, color Doppler flow imaging; HE, hematoxylin and eosin.

Multimodal ultrasound features associated with SA and IDC

Compared with IDC, the calcification (χ^2=20.878, P<0.001) and retraction phenomenon in the coronal planes (χ^2=18.888; P<0.001) were less common in SA; circumscribed margin (χ^2=18.151; P<0.001), vascularity grade 0–I (χ^2=23.231; P<0.001), and elasticity scores 1–3 (χ^2=43.883; P<0.001) were more common in SA, and significant differences were found between the two group. Patients with SA were significantly younger than those with IDC (*t*=–5.557; P<0.001), and the lesion size was smaller in SA than in IDC (*t*=–3.663; P<0.001). The multimodal ultrasound features and histopathological characteristics of SA or IDC are summarized in *Figures 2,3*. The distribution of multimodal ultrasound features between the two groups is presented in *Table 1*.

Diagnostic performances of ABVS, EI, CDFI, and their combination in differentiating SA from IDC

The ROC curve analysis of ABVS, EI, CDFI and their combination was conducted, and the results are shown in *Figure 4*. There was no significant difference in the diagnostic efficacy between each pair of methods (ABVS *vs.* EI, P=0.266; ABVS *vs.* CDFI, P=0.4671; EI *vs.* CDFI, P=0.051), while the diagnostic efficacy of the combined model was significantly higher than that of the three imaging methods (ABVS *vs.* combined model, P<0.001; CDFI *vs.* combined model, P<0.001; EI *vs.* combined model, P<0.001). The diagnostic performances of ABVS, EI, CDFI, and their combination are presented in *Table 2*.

Discussion

In this study, multimodal ultrasound imaging was employed for the differential diagnosis of SA and IDC. The combination of ABVS, EI, and CDFI exhibited an optimal diagnostic accuracy, with an AUC of 0.895 [95% confidence interval (CI): 0.827–0.943], which was significantly higher than that of the three imaging methods (P<0.05). This indicated the superiority of multimodal

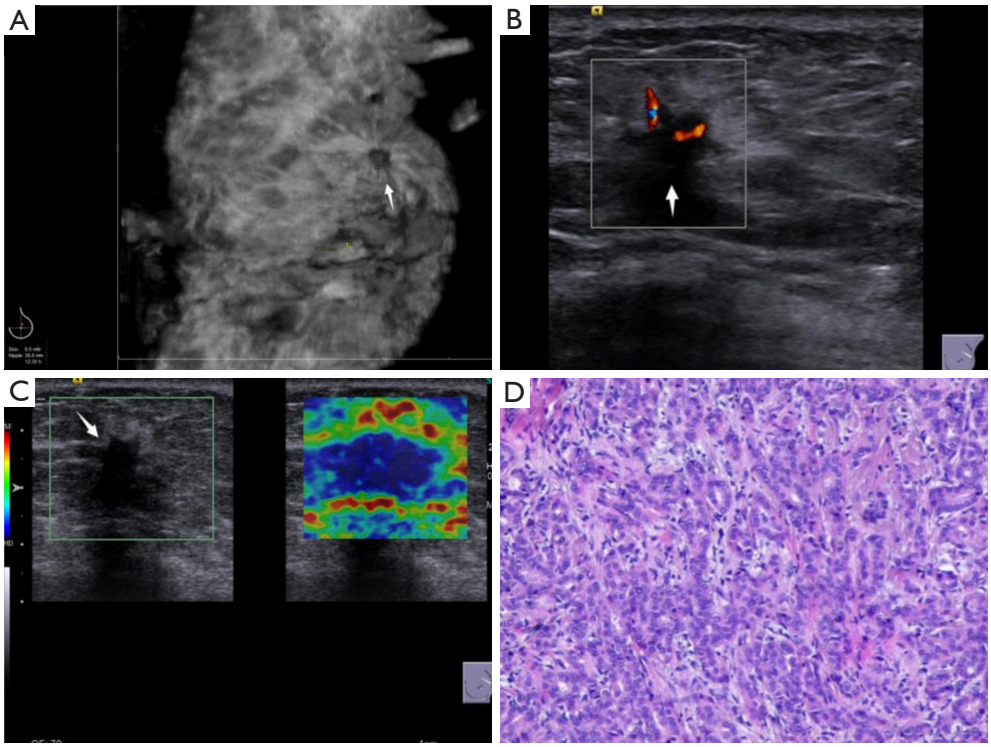

Figure 3 Pictures shows the imaging and histopathology findings of a case of invasive ductal carcinoma. (A) An IDC lesion (white arrow) with an irregular shape, no circumscribed margin, and retraction phenomenon in the coronal planes. (B) CDFI shows a lesion (white arrow) with advanced central blood flow (vascularity grade III). (C) The lesion's (white arrow) elasticity imaging shows dark blue due to high stiffness with an elasticity score of 5 points. (D) HE staining showing an IDC lesion with diffuse cords and nests of pleomorphic tumor cells, predominated by nucleoli and numerous mitoses (HE staining; original magnification, 100×). IDC, invasive ductal carcinoma; CDFI, color Doppler flow imaging; HE, hematoxylin and eosin.

ultrasound imaging in the differential diagnosis of SA and IDC. The diagnostic sensitivity and specificity could increase to 88.24% and 74.07%, respectively. The results indicated that the combined application not only improved the diagnosis of IDC but also reduced the unnecessary biopsy of SA. To date, few studies have concentrated on differentiating SA from IDC using multimodal ultrasound imaging. Liu *et al.* (14) demonstrated that utilization of conventional ultrasound combined with breast elastography could be a promising approach to differentiating SA from breast cancer. To best of our knowledge, no study has indicated the diagnostic efficiency. Chen *et al.* (6) found that the integrated application of ABVS, MG, and MRI could improve the preoperative evaluation of SA, while the analyzed masses were SA lesions associated with malignant or benign lesions. To our knowledge, this is the first multicenter study to employ multimodal ultrasound imaging (ABVS, EI, and CDFI) for distinguishing SA from IDC.

ABVS is a three-dimensional breast imaging modality, which can simultaneously provide morphological features in the transverse, sagittal, and coronal planes (19). Chen *et al.* (7) used conventional ultrasound for diagnosing SA, which yielded an AUC of 0.55, which was lower than that of ABVS achieved in our study (0.55 *vs.* 0.736). This could be related to the fact that the coronal plane is exclusive to ABVS and inaccessible to conventional ultrasound. The retraction phenomenon could be found in the coronal plane, which has been described to have a superior 100.0% specificity and 80.0% sensitivity in detecting breast cancer, with a high 91.4% accuracy in differentiating malignant lesions from benign lesions (20). In our study, SA exhibited a significantly less likelihood of demonstrating the retraction phenomenon in the coronal planes than did IDC ($P<0.05$), which is consistent with Chen *et al.*'s findings (6). Of note, the occurrence rate of the retraction

Table 1 Multimodal ultrasound imaging features of patients with SA and patients with IDC

Baseline variables	SA (n=54)	IDC (n=68)	$c^2/t/Z$	P
Age (years)	43±11	54±11	–5.557	<0.001
Size (cm)	1.0 (0.9)	1.3 (1.3)	–3.663	<0.001
Shape			2.570	0.109
Regular	9 (16.67)	5 (7.35)		
Irregular	45 (83.33)	63 (92.65)		
Orientation			0.029	0.865
Parallel	42 (77.78)	52 (76.47)		
Not parallel	12 (22.22)	16 (23.53)		
Margin			18.151	<0.001
Circumscribed	21 (38.89)	4 (5.88)		
Not circumscribed	33 (61.11)	64 (94.12)		
Echo pattern			1.706	0.192
Homogeneity	12 (22.22)	9 (13.24)		
Heterogeneity	42 (77.78)	59 (86.76)		
Calcification			20.878	<0.001
In a mass	9 (16.67)	39 (57.35)		
None	45 (83.33)	29 (42.65)		
Posterior feature			0.550	0.752
No posterior feature	41 (75.93)	48 (70.59)		
Enhancement sound	2 (3.70)	4 (5.88)		
Shadowing	11 (20.37)	16 (23.53)		
Vascularity grade			23.231	<0.001
Grade 0–I	35 (64.81)	18 (26.47)		
Grade II–III	19 (35.19)	50 (73.53)		
Retraction phenomenon on the coronal planes			18.888	<0.001
No	44 (81.48)	29 (42.65)		
Yes	10 (18.52)	39 (57.35)		
Elasticity scores			43.883	<0.001
Score 1–3	39 (72.22)	9 (13.24)		
Score 4–5	15 (27.78)	59 (86.76)		

Data are shown as mean ± standard deviation or n (%). SA, sclerosing adenosis; IDC invasive ductal carcinoma.

phenomenon in SA was 18.52% in the coronal plane as achieved by ABVS, which could be mainly related to the growth of stoma fiber hyperplasia in adjacent glands and fat tissue forming the "pseudo infiltration" (21). Distinguishing SA from IDC is a diagnostic challenge, and pathological evaluation should be carried out for final diagnosis. A previous study (22) demonstrated that using ABVS has an excellent accuracy in distinguishing benign lesions from

malignant breast lesions, with a sensitivity between 89.9% and 93.8% and a specificity between 82.4% and 87%, which are higher than the values achieved in our study (sensitivity 75.00%, specificity 72.22%). This could be related to the type of lesions that were analyzed in our study. ABVS was previously used to evaluate all types of breast lesions, while only SA and IDC lesions were assessed in our study. The characteristics of SA and IDC typically lead to misdiagnosis, and it is difficult to differentiate them only via ABVS (6).

Notably, EI and CDFI can act as potent complementary tools in the diagnostic process for complex SA, especially when there are multiple imaging symptoms simulating malignancy in grayscale ultrasound (11,23). For the diagnosis of breast lesions, two types of elastography are currently adopted: strain elastography (SE) and shear wave elastography (SWE). SWE offers quantitative values for the Young elastic modulus (in kilopascals) of tissues by imaging shear wave propagation (24). SWE has demonstrated high inter- and intraobserver reproducibility for both qualitative and quantitative parameters (25); however, there is no standard optimal diagnostic cutoff value for distinguishing between benign and malignant breast lesions. Several strain imaging parameters have been used to differentiate between benign and malignant breast lesions. The most prevalent variables are the elasticity score (a color map of stiffness), the elasticity to B (E/B) mode ratio (width ratio or length ratio), and the strain ratio [fat-to-lesion ratio (FLR)], which have been shown to be of favorable value in distinguishing benign from malignant breast lesions (26). The elasticity value can clearly show the borderline of the breast lesions, particularly for those lesions that cannot be easily differentiated from their surrounding tissues or even for some deeply located lesions that cannot be detected in clinical palpation (14). In our study, the elasticity score of SA was generally 1–3 points, while the elasticity score of IDC was typically 4–5 points, which was consistent with Wang *et al.*'s findings (18), who considered a score of 3 as a diagnostic cutoff value. When the lesion elasticity score was greater than or equal to 3, it was classified as malignant, while lesions with a score less than 3 were classified as benign. The results of the present study indicated that for distinguishing SA from IDC, the sensitivity, specificity, and accuracy of EI were 86.76%, 72.22%%, and 80.33%, respectively. These results are comparable to those of previous studies (27,28), which reported a 76.10–83.7% sensitivity and a 69.90–93.70% specificity.

There is an obvious distinction in vascular architecture between benign and malignant tumors (29). CDFI, as one of the most widely used ultrasound techniques, provides valuable data for evaluating blood flow, which can eliminate

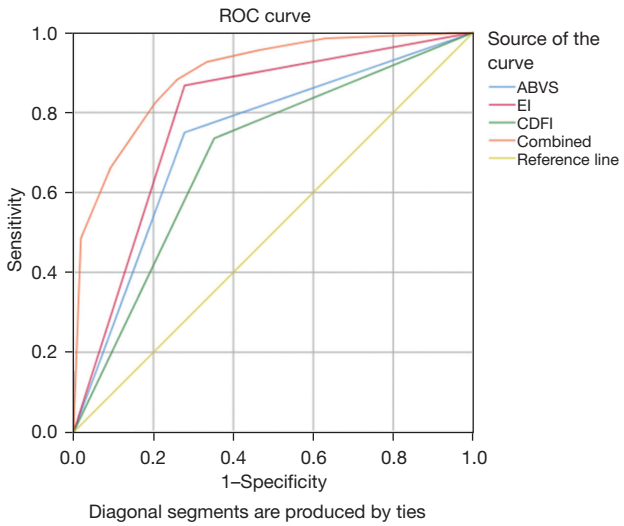

Figure 4 ROC curve analysis of SA and IDC diagnosed with ABVS, EI, CDFI, and their combination. ROC, receiver operating characteristic; SA, sclerosing adenosis; IDC, invasive ductal carcinoma; ABVS, automated breast volume scan; EI, elasticity imaging; CDFI, color Doppler flow imaging; combined, combination of ABVS, EI, and CDFI.

Table 2 Diagnostic performances of ABVS, EI, CDFI, and their combination

Method	Sensitivity (%)	Specificity (%)	Accuracy (%)	AUC (95% CI)
ABVS	75.00 (51/68)	72.22 (39/54)	73.77 (90/122)	0.736 (0.649–0.812)
EI	86.76 (59/68)	72.22 (39/54)	80.33 (98/122)	0.795 (0.712–0.863)
CDFI	73.53 (50/68)	64.81 (35/54)	69.67 (85/122)	0.692 (0.602–0.772)
Combined modality	88.24 (60/68)	74.07 (40/54)	81.97 (100/122)	0.895 (0.827–0.943)

ABVS, automated breast volume scan; EI, elasticity imaging; CDFI, color Doppler flow imaging; combined modality, combination of ABVS, EI, and CDFI; AUC, area under the curve; CI, confidence interval.

the defects of ABVS, as ABVS cannot indicate the blood flow characteristics of the breast lesions (30). In the present study, regarding the differential diagnosis of SA and IDC, the sensitivity and specificity of CDFI were 73.53% and 64.81%, respectively. The diagnostic value of using CDFI alone to distinguish SA from IDC was limited, which was consistent with Ma *et al.*'s findings (31), who demonstrated that the differentiation of benign and malignant breast lesions by CDFI can be restricted by its angular dependency and poor signal-to-noise ratios. Additionally, it is typically unable to evaluate flow signals from small vessels (<1 mm) when the flow rate is low (3–5 cm/s).

In very recent articles, there is a controversy concerning the added value of using a gel stand-off pad and high frequency probes (>15 MHz) to better document the vascularization of breast lesions (32,33). The use of a gel stand-off pad serves to augment the separation between the transducer and the intended object, thereby facilitating the alignment of the object within the optimal focal region. This alignment results in the maximization of axial resolution at the specific depth where the operator manually positions the focus (34). Therefore, the use of a gel stand-off pad enables the attainment of a presumptive or definitive diagnosis for superficial lesions while also enhancing the detection of additional flow signals within small cutaneous nodules.

Since the beginning of the 1980s, there have been numerous reports on the use of high-frequency sonography for skin examination. Over time, advancements in technology have facilitated the integration of ultrasound as a valuable tool in clinical examinations for a wide range of indications. Notably, the introduction of 20-MHz probes has contributed substantially in this development (32). Corvino *et al.* (33) showed that the high-frequency probe can better visualize the vascularization, nipple-areolar complex abnormalities, and superficial breast parenchyma abnormalities of breast lesions. Thus, ideally, two multifrequency linear probes should be available to perform breast examinations, one with a frequency range from 7.5 to 14 MHz (as suggested by American College of Radiology) and another with an upper frequency of 15 to 24 MHz. Given its higher penetration, the former transducer is necessary to explore the deeper layers (muscle plane, the fascia, the retromammary layer) and the lesions of considerable size and the vascularization, while the latter one, due to the higher resolution, allows for improved anatomical detail.

In thus study, the mean age of patients with SA was 43 years old, which was consistent with Chen *et al.*'s results (7), and SA may occur in all age groups, but especially in perimenopausal women aged 40–50 years. Our study revealed that patients with SA were significantly younger than those with IDC, which was consistent with previously reported findings (21). The calcification and retraction phenomena in the coronal planes were less frequently observed in patients with SA than in patients with IDC. Circumscribed margin, vascularity grade 0–I, and elasticity scores 1–3 were more frequently observed in patients with SA than in those with IDC and constituted a statistically significant differences between these two groups. Moreover, the lesion size in the SA group was significantly smaller than that in the IDC group. Exploration of the imaging features of SA and their careful assessment will be advantageous in its differential diagnosis.

This study was subject to various limitations. First, we employed a retrospective, single-center design, and it is important to note that the sample size was limited. Therefore, it is recommended that future research includes larger sample sizes and involves multiple centers to enhance the generalizability of the findings. Furthermore, it should be mentioned that only multimodal ultrasound images were incorporated in the analysis of all patients, whereas MG and MRI were not included. The potential absence of data pertaining to MG and MRI could lead to an inadequate assessment. Moreover, SA predominantly manifests in conjunction with both benign and malignant neoplasms of the breast. Due to the potential difficulties in accurately diagnosing malignant lesions associated with SA, additional comprehensive investigations are necessary to investigate a broader range of imaging resources for this complex condition.

Conclusions

In summary, the combined use of ABVS, EI, and CDFI in the assessment of breast lesions has demonstrated superior diagnostic efficacy compared to each method used in isolation. Furthermore, this combined approach offers additional insights into distinguishing between SA and IDC in the differential diagnostic process.

Acknowledgments

The authors are grateful for the support and help of department of Radiology, the First Affiliated Hospital of Soochow University, and all the staff at the Department of Ultrasound, Huadong Sanatorium.

Funding: This study was supported by the Gusu Medical Talent of Suzhou City Program (grant No. GSWS2020009), the Translational Research Grant of NCRCH (grant No. 2020WSB06), and the Jiangsu Provincial Key Medical Discipline (grant No. JSDW202242).

Footnote

Reporting Checklist: The authors have completed the STARD reporting checklist. Available at https://qims.amegroups.com/article/view/10.21037/qims-23-524/rc

Conflicts of Interest: All authors have completed the ICMJE uniform disclosure form (available at https://qims.amegroups.com/article/view/10.21037/qims-23-524/coif). Y.L. reports that this study was supported by the Gusu Medical Talent of Suzhou City Program (grant No. GSWS2020009), the Translational Research Grant of NCRCH (grant No. 2020WSB06), and the Jiangsu Provincial Key Medical Discipline (grant No. JSDW202242). The other authors have no conflicts of interest to declare.

Ethical Statement: The authors are accountable for all aspects of the work in ensuring that questions related to the accuracy or integrity of any part of the work are appropriately investigated and resolved. The study was conducted in accordance with the Declaration of Helsinki (as revised in 2013). The study was approved by the Institutional Review Board of the Huadong Sanatorium (approval No. ECHS2023-09). Individual consent for this retrospective analysis was waived.

References

1. Tan H, Zhang H, Lei Z, Fu F, Wang M. Radiological and clinical findings in sclerosing adenosis of the breast. Medicine (Baltimore) 2019;98:e17061.
2. Cui X, Wei S. Carcinoma In Situ Involving Sclerosing Adenosis: Seeking the Salient Histological Characteristics to Prevent Overdiagnosis. Ann Clin Lab Sci 2017;47:529-34.
3. Shoker BS, Jarvis C, Clarke RB, Anderson E, Munro C, Davies MP, Sibson DR, Sloane JP. Abnormal regulation of the oestrogen receptor in benign breast lesions. J Clin Pathol 2000;53:778-83.
4. Rosa M, Agosto-Arroyo E. Core needle biopsy of benign, borderline and in-situ problematic lesions of the breast: Diagnosis, differential diagnosis and immunohistochemistry. Ann Diagn Pathol 2019;43:151407.
5. Nakhlis F, Lester S, Denison C, Wong SM, Mongiu A, Golshan M. Complex sclerosing lesions and radial sclerosing lesions on core needle biopsy: Low risk of carcinoma on excision in cases with clinical and imaging concordance. Breast J 2018;24:133-8.
6. Chen H, Bao L, Yu L, Sun H, Tan Y, Wei P, Zheng Z. Value of multimodal imaging in the diagnosis of breast sclerosing adenosis associated with malignant lesions. J Clin Ultrasound 2023;51:485-93.
7. Chen YL, Chen JJ, Chang C, Gao Y, Wu J, Yang WT, Gu YJ. Sclerosing adenosis: Ultrasonographic and mammographic findings and correlation with histopathology. Mol Clin Oncol 2017;6:157-62.
8. Hao W, Gong J, Wang S, Zhu H, Zhao B, Peng W. Application of MRI Radiomics-Based Machine Learning Model to Improve Contralateral BI-RADS 4 Lesion Assessment. Front Oncol 2020;10:531476.
9. Axmacher JA, Bhatt AA, Hesley GK. Nodular sclerosing adenosis detected as focal uptake on molecular breast imaging. Radiol Case Rep 2020;15:1211-5.
10. Durmus T, Stöckel J, Slowinski T, Thomas A, Fischer T. The hyperechoic zone around breast lesions - an indirect parameter of malignancy. Ultraschall Med 2014;35:547-53.
11. Lee SH, Chung J, Choi HY, Choi SH, Ryu EB, Ko KH, Koo HR, Park JS, Yi A, Youk JH, Son EJ, Chu AJ, Chang JM, Cho N, Jang MJ, Kook SH, Cha ES, Moon WK. Evaluation of Screening US-detected Breast Masses by Combined Use of Elastography and Color Doppler US with B-Mode US in Women with Dense Breasts: A Multicenter Prospective Study. Radiology 2017;285:660-9.
12. Wang J, Fan H, Zhu Y, Shen C, Qiang B. The value of automated breast volume scanner combined with virtual touch tissue quantification in the differential diagnosis of benign and malignant breast lesions: A comparative study with mammography. Medicine (Baltimore) 2021;100:e25568.
13. Li XL, Lu F, Zhu AQ, Du D, Zhang YF, Guo LH, Sun LP, Xu HX. Multimodal Ultrasound Imaging in Breast

Imaging-Reporting and Data System 4 Breast Lesions: A Prediction Model for Malignancy. Ultrasound Med Biol 2020;46:3188-99.
14. Liu W, Li W, Li Z, Shi L, Zhao P, Guo Z, Tian J, Wang Z. Ultrasound characteristics of sclerosing adenosis mimicking breast carcinoma. Breast Cancer Res Treat 2020;181:127-34.
15. Tessler FN, Middleton WD, Grant EG, Hoang JK, Berland LL, Teefey SA, Cronan JJ, Beland MD, Desser TS, Frates MC, Hammers LW, Hamper UM, Langer JE, Reading CC, Scoutt LM, Stavros AT. ACR Thyroid Imaging, Reporting and Data System (TI-RADS): White Paper of the ACR TI-RADS Committee. J Am Coll Radiol 2017;14:587-95.
16. Tozaki M, Fukuma E. Category assessment based on 3D volume data acquired by automated breast ultrasonography. Jpn J Radiol 2012;30:185-91.
17. Adler DD, Carson PL, Rubin JM, Quinn-Reid D. Doppler ultrasound color flow imaging in the study of breast cancer: preliminary findings. Ultrasound Med Biol 1990;16:553-9.
18. Wang Z, Liu N, Zhang L, Li X, Han X, Peng Y, Dang M, Sun L, Tian J. Real-Time Elastography Visualization and Histopathological Characterization of Rabbit Atherosclerotic Carotid Arteries. Ultrasound Med Biol 2016;42:176-84.
19. Wang SJ, Liu HQ, Yang T, Huang MQ, Zheng BW, Wu T, Qiu C, Han LQ, Ren J. Automated Breast Volume Scanner (ABVS)-Based Radiomic Nomogram: A Potential Tool for Reducing Unnecessary Biopsies of BI-RADS 4 Lesions. Diagnostics (Basel) 2022.
20. Lin X, Wang J, Han F, Fu J, Li A. Analysis of eighty-one cases with breast lesions using automated breast volume scanner and comparison with handheld ultrasound. Eur J Radiol 2012;81:873-8.
21. Li C, Zhang H, Chen J, Shao S, Li X, Yao M, Zheng Y, Wu R, Shi J. Deep learning radiomics of ultrasonography for differentiating sclerosing adenosis from breast cancer. Clin Hemorheol Microcirc 2023;84:153-63.
22. Meng Z, Chen C, Zhu Y, Zhang S, Wei C, Hu B, Yu L, Hu B, Shen E. Diagnostic performance of the automated breast volume scanner: a systematic review of inter-rater reliability/agreement and meta-analysis of diagnostic accuracy for differentiating benign and malignant breast lesions. Eur Radiol 2015;25:3638-47.
23. Kanagaraju V, Dhivya B, Devanand B, Maheswaran V. Utility of Ultrasound Strain Elastography to Differentiate Benign from Malignant Lesions of the Breast. J Med Ultrasound 2021;29:89-93.
24. Faruk T, Islam MK, Arefin S, Haq MZ. The Journey of Elastography: Background, Current Status, and Future Possibilities in Breast Cancer Diagnosis. Clin Breast Cancer 2015;15:313-24.
25. Dhyani M, Anvari A, Samir AE. Ultrasound elastography: liver. Abdom Imaging 2015;40:698-708.
26. Sigrist RMS, Liau J, Kaffas AE, Chammas MC, Willmann JK. Ultrasound Elastography: Review of Techniques and Clinical Applications. Theranostics 2017;7:1303-29.
27. Zheng X, Huang Y, Wang Y, Liu Y, Li F, Han J, Wang J, Cao L, Zhou J. Combination of different types of elastography in downgrading ultrasound Breast Imaging-Reporting and Data System category 4a breast lesions. Breast Cancer Res Treat 2019;174:423-32.
28. Han J, Li F, Peng C, Huang Y, Lin Q, Liu Y, Cao L, Zhou J. Reducing Unnecessary Biopsy of Breast Lesions: Preliminary Results with Combination of Strain and Shear-Wave Elastography. Ultrasound Med Biol 2019;45:2317-27.
29. Zhu YC, Zhang Y, Deng SH, Jiang Q. Diagnostic Performance of Superb Microvascular Imaging (SMI) Combined with Shear-Wave Elastography in Evaluating Breast Lesions. Med Sci Monit 2018;24:5935-42.
30. Zhu YC, Zu DM, Zhang Y, Shan J, Shi XR, Deng SH, Jiang Q. A comparative study on superb microvascular imaging and conventional ultrasonography in differentiating BI-RADS 4 breast lesions. Oncol Lett 2019;18:3202-10.
31. Ma Y, Li G, Li J, Ren WD. The Diagnostic Value of Superb Microvascular Imaging (SMI) in Detecting Blood Flow Signals of Breast Lesions: A Preliminary Study Comparing SMI to Color Doppler Flow Imaging. Medicine (Baltimore) 2015;94:e1502.
32. Corvino A, Sandomenico F, Corvino F, Campanino MR, Verde F, Giurazza F, Tafuri D, Catalano O. Utility of a gel stand-off pad in the detection of Doppler signal on focal nodular lesions of the skin. J Ultrasound 2020;23:45-53.
33. Corvino A, Varelli C, Catalano F, Cocco G, Delli Pizzi A, Boccatonda A, Corvino F, Basile L, Catalano O. Use of High-Frequency Transducers in Breast Sonography. J Pers Med 2022;12:1960.
34. Corvino A, Corvino F, Catalano O, Sandomenico F, Petrillo A. The Tail and the String Sign: New Sonographic Features of Subcutaneous Melanoma Metastasis. Ultrasound Med Biol 2017;43:370-4.

Cite this article as: Li W, Zheng Y, Liu H, Tai Z, Zhu H, Li Z, Gu Q, Li Y. Multimodal ultrasound imaging for diagnostic differentiation of sclerosing adenosis from invasive ductal carcinoma. Quant Imaging Med Surg 2024;14(1):877-887. doi: 10.21037/qims-23-524

